Noninvasive Monitoring of Murine Tumor Blood Flow During and After Photodynamic Therapy Provides Early Assessment of Therapeutic Efficacy

Guoqiang Yu,[1] Turgut Durduran,[1] Chao Zhou,[1] Hsing-Wen Wang,[1,2] Mary E. Putt,[3] H. Mark Saunders,[4] Chandra M. Sehgal,[5] Eli Glatstein,[2] Arjun G. Yodh,[1] and Theresa M. Busch[2]

Abstract

Purpose: To monitor tumor blood flow noninvasively during photodynamic therapy (PDT) and to correlate flow responses with therapeutic efficacy.

Experimental Design: Diffuse correlation spectroscopy (DCS) was used to measure blood flow continuously in radiation-induced fibrosarcoma murine tumors during Photofrin (5 mg/kg)/ PDT (75 mW/cm^2, 135 J/cm^2). Relative blood flow (rBF; i.e., normalized to preillumination values) was compared with tumor perfusion as determined by power Doppler ultrasound and was correlated with treatment durability, defined as the time of tumor growth to a volume of 400 mm^3. Broadband diffuse reflectance spectroscopy concurrently quantified tumor hemoglobin oxygen saturation (SO$_2$).

Results: DCS and power Doppler ultrasound measured similar flow decreases in animals treated with identical protocols. DCS measurement of rBF during PDT revealed a series of PDT-induced peaks and declines dominated by an initial steep increase (average $\pm$ SE: 168.1 $\pm$ 39.5%) and subsequent decrease (59.2 $\pm$ 29.1%). The duration (interval time; range, 2.2-15.6 minutes) and slope (flow reduction rate; range, 4.4 -45.8% minute^{-1}) of the decrease correlated significantly ($P = 0.0001$ and 0.0002, $r^2 = 0.79$ and 0.67, respectively) with treatment durability. A positive, significant ($P = 0.016$, $r^2 = 0.50$) association between interval time and time-to-400 mm^3 was also detected in animals with depressed pre-PDT blood flow due to hydralazine administration. At 3 hours after PDT, rBF and SO$_2$ were predictive ($P \leq 0.015$) of treatment durability.

Conclusion: These data suggest a role for DCS in real-time monitoring of PDT vascular response as an indicator of treatment efficacy.

Photodynamic therapy (PDT; ref. 1) requires administration of a photosensitizer that localizes in tumor tissue and is subsequently activated by exposure to optical radiation. The photo-excited photosensitizer initiates a cascade of chemical reactions, involving highly reactive oxygen intermediates that can cause necrosis and apoptosis of cells (2), activation of the host immune system (3), and vascular damage (4). The antivascular effects of PDT are an important component of tissue response to treatment. The extent of PDT-created vascular damage is determined by a number of factors, including the photosensitizer and its dose (5 – 7), the interval between

The costs of publication of this article were defrayed in part by the payment of page charges. This article must therefore be hereby marked *advertisement* in accordance with 18 U.S.C. Section 1734 solely to indicate this fact.
Requests for reprints: Guoqiang Yu, David Rittenhouse Laboratory, Department of Physics and Astronomy, 209 South 33rd Walnut Street, Philadelphia, PA 19104. Phone: 215-573-3463; Fax: 215-573-6391; E-mail: guoqiang@physics. upenn.edu.

photosensitizer injection and tumor illumination (4, 8), and the total fluence and fluence rate of treatment (9 – 11).

Numerous studies suggest that PDT-mediated vascular damage significantly contributes to long-term tumor response. In one investigation, murine tumors regrew rapidly when PDT was combined with inhibition of thromboxane, a mediator of platelet adhesion and vasoconstriction (12). Conversely, enhancement of tumor vascular damage by inhibition of nitric oxide synthase after Photofrin-PDT increased the cure rate of murine tumors (13).

The time course of PDT antivascular effects is crucial. The collapse of tumor microvessels after PDT is beneficial, leading to local anoxia and nutrient deprivation of tumor cells (9). However, the induction of temporary vasoconstriction or obstruction during PDT may lead to regional tissue hypoxia during illumination (14) and thus be a barrier to effective treatment. Given the dichotomy of these effects, knowledge of the timing of vascular shutdown in PDT-treated tissues holds potential as a useful indicator of therapeutic efficacy.

There are a number of techniques for measuring the blood flow of tumors. Laser Doppler can noninvasively monitor the flow change, but most systems measure only the tissue surface (penetration depth <500 μm; refs. 15, 16). Pogue et al. have invasively monitored flow changes during PDT with laser Doppler using fiber probes inserted into tumors (17). Their work suggests that the irradiation light saturates the Doppler

probe, yielding useful data only between light fractions. Optical coherence tomography has high spatial and temporal resolution, permitting the imaging of local vascular changes (18, 19). However, optical coherence tomography can only measure small near-surface tissue volumes (~ 1 mm^2; ref. 20), similar to the laser Doppler technique. Power Doppler ultrasound can noninvasively follow changes in tumor perfusion after PDT through determination of the color-weighed fractional area in acquired images (21). However, it does not readily allow continuous measurement during PDT.

Near-IR diffuse correlation spectroscopy (DCS) enables measurement of rBF noninvasively through deep tissues. It has been successfully applied and validated in studies of functional imaging and spectroscopy of brain (22–24), tumor physiology (25), tissue burns (26), and exercise medicine (27, 28). DCS is closely related to the commonly used laser Doppler technology, but it offers the advantage of deeper measurement through tissues. Furthermore, with appropriate optical cutoff filters, DCS can be used to follow tumor blood flow continuously during PDT.

In this study, we employed a DCS system and a unique noncontact probe to monitor the rBF of murine tumors during illumination for Photofrin-PDT and at specific time points after treatment. Within minutes of beginning PDT, rBF rapidly increased, followed by a decline and subsequent peaks and declines of various kinetics. The slope (flow reduction rate) and duration (interval time) over which rBF decreased following the initial PDT-induced increase was highly associated with treatment durability; treatment durability is measured as the time of tumor growth to a volume of 400 mm^3 (time-to-400 mm^3). After PDT, all animals showed decreases in rBF at 3 and 6.5 hours, and rBF at these time points was also predictive of tumor response. Broadband diffuse reflectance spectroscopy was employed to measure the tissue hemoglobin oxygen saturation (SO$_2$) of the PDT-treated tumors, finding that SO$_2$ decreased after PDT in association with the decreases in rBF. These data show that DCS-measured changes in tumor rBF during and after Photofrin-PDT are predictive of treatment efficacy.

Materials and Methods

Tumor model and photodynamic therapy. Radiation-induced fibrosarcoma tumors were propagated on the shoulders of C3H mice (Taconic, Germantown, NY) by the intradermal injection of 3×10^5 cells. Animals were treated ~ 1 week later when tumors were ~ 6 to 7 mm in diameter. The photosensitizer Photofrin (Axcan Pharma, Inc., Mont-Saint-Hilaire, Quebec) was given via tail vein at 5 mg/kg at ~ 24 hours before illumination. The laser system consisted of a KTP YAG pumped dye module (Laserscope, San Jose, CA) tuned to produce 630 nm light. Light was delivered to a 1-cm-diameter treatment field through microlens-tipped fibers (CardioFocus, Norton, MA) and the power density was measured with a power meter (Coherent, Auburn, CA). Treatment was to a total fluence of 135 J/cm^2, delivered at 75 mW/cm^2. Treatment groups consisted of animals receiving PDT ($n = 15$) and animals receiving light but no Photofrin ($n = 10$). To alter blood flow in a manner independent of PDT, an additional 11 animals received an i.v. injection (2.5 or 5.0 mg/kg in saline) of hydralazine (Sigma Aldrich, St. Louis, MO) at 10 minutes before beginning illumination. During illumination and during optical measurement, mice were anesthetized with isoflurane and kept warm on a heating pad. Treatment durability was measured as the number of days after PDT or after control treatment until tumor growth to a

volume of 400 mm^3 (tumor volume = length $\times$ width$^2 \times 3.14/6$; i.e., time-to-400 mm^3).

Diffuse correlation spectroscopy. DCS was used to monitor blood flow continuously during PDT (from 10 minutes before PDT until 15 minutes after PDT) and for 10-minute durations at times 3 and 6.5 hours after PDT. In animals that received hydralazine, blood flow monitoring began 10 minutes before hydralazine injection and continued another 10 minutes preillumination, 30 minutes of illumination, and 15 minutes after PDT. A 3-hour time point was also evaluated in mice treated with hydralazine and PDT. The major components (25) of the DCS system are the following: an 800-nm laser source with long coherence length, operating in continuous mode; a noncontact probe with 13 source and four detector fibers; and a camera to deliver excitation light and collect reflected diffuse light, respectively (Fig. 1A), from the tissue surface. The noncontact probe (Fig. 1B) consists of 13 source fibers arranged in concentric circles within a 6-mm diameter. Using optical switches, the 800-nm light was directed through each of the source fibers in a consecutive manner; the sampling time for one scanning frame (i.e., all source-detector pairs) was 18 seconds. Four single photon–counting avalanche photodiodes were employed in parallel for detection of the diffuse light. The probe head was mounted behind a camera lens fixed at a distance of 15 cm from the tumor. This setup enabled us to monitor blood flow during PDT by permitting unobstructed illumination with the treatment light at a small angle to the tissue surface. A long-pass optical filter (03FCG 507, Melles Griot, Rochester, NY) in front of the camera lens attenuated light below 650 nm, preventing the 630-nm treatment light from saturating the detectors.
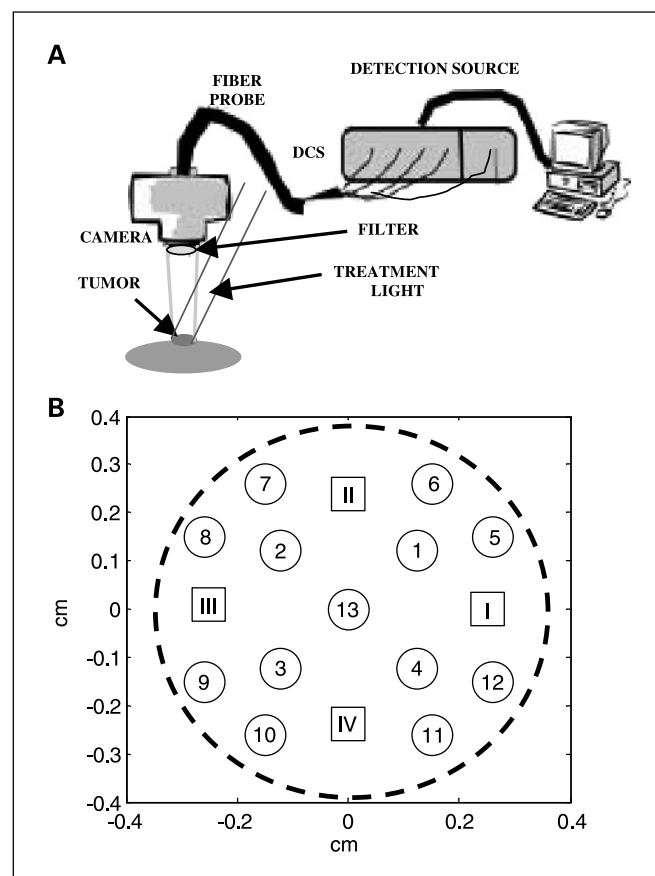
Fig. 1. A schematic of the DCS instrument (*A*) and a map (*B*) of the probe for measuring tumor blood flow. Optical fibers for 13 source positions (*small circles*) and four DCS detectors (*squares*) are arranged in a two-dimensional pattern. *Large dashed circle*, contour of the tumor.

Speckle fluctuations of the diffuse light are sensitive to the motions of tissue scatterers such as red blood cells. The quantity containing this information is the electric field ($E(r,t)$) (26). The electric field temporal autocorrelation function, $G_1(r,\tau) = \langle E(r,t)\ E^*(r,t+\tau)\rangle$, or its Fourier Transform can be explicitly related to the motion of the scatterers (e.g., red blood cells) even in turbid media (29–31). Here the angle brackets $\langle\ \rangle$ denote averages over time and τ is called the correlation delay time. A continuous wave laser with a long coherence length and a single-photon counting avalanche photodiode are needed for DCS measurements. An autocorrelator takes the avalanche photodiode output and uses photon arrival times to compute the light intensity temporal autocorrelation function. From the normalized intensity autocorrelation function, we calculate the normalized electric field correlation function, $g_1(r,\tau) = G_1(r,\tau)/\langle E(r,t)\ E^*(r,t)\rangle$; $G_1(r,\tau)$, satisfies the correlation diffusion equation in highly scattering media (26, 31). The exact form of the correlation diffusion equation depends on the nature and heterogeneity of the particle motion. For the important case of random flow in the tissue vasculature, the mean-square displacement, $(\langle\Delta r^2(\tau)\rangle)$, of the scattering particles (e.g., blood cells) in time τ is $\langle\Delta r(\tau)\rangle = \langle V^2\rangle\tau^2$. Here $\langle V^2\rangle$ is the second moment of the cell velocity distribution. For the case of diffusive motion, $\langle\Delta r^2(\tau)\rangle = 6D_B\tau$, where D_B is an effective diffusion coefficient of the moving scatterers. We have found that both of these models fit our data, but the latter model often provides better quality fits (23). In this case the normalized correlation function $g_1(r,\tau)$ will decay approximately exponentially in τ. Its decay depends on a variable α (proportional to the tissue blood volume fraction) and on the mean-square displacement of the blood cells. Relative changes in D_B or $\sqrt{\langle V^2\rangle}$ are correlated with relative changes in blood flow. In principle, DCS can measure absolute levels of blood flow. In practice, however, it is desirable to calibrate DCS with other measurement techniques (e.g., Arterial Spin Label magnetic resonance imaging, ultrasound Doppler, etc.) for quantification of absolute flow. In this study, only *relative* blood flow is reported, and these relative blood flow changes are *insensitive* to our model for $\langle\Delta r^2(\tau)\rangle$ (i.e., the relative change of D_B and $\sqrt{\langle V^2\rangle}$ are almost identical). A detailed description of these concepts and approximations can be found in the noted references (22, 23), and a comparison with Power Doppler ultrasound will be provided in this article.

DCS reflects local flow in primarily small vessels (i.e., arterioles, capillaries, and venules). From diffusion theory, the maximum penetration depth of diffuse light in tissue depends on tissue optical properties and source-detector separation. The most probable penetration depth of diffuse light in tissue is roughly one third to one half of the source-detector separation on the tissue surface. Therefore, a specific source-detector pair predominately provides information about a particular tissue layer. The source-detector separations used in this study ranged from 1 to 3.5 mm, providing flow information from depths of 0.5 to 1.7 mm. We found the magnitude of PDT effect on rBF differed with tumor depth, although the trends were similar among tumor layers. In this study, DCS data for one scanning frame were averaged over all source-detector separations (1-3.5 mm), representing the rBF in the bulk tumor tissue. rBF at 3 and 6.5 hours were obtained by averaging over 10 minutes of monitoring. rBF during PDT was characterized by the variables of a linear regression model fit to the first treatment-induced decrease in flow. The SE of the slope and intercept of the linear model represent the fitting errors in flow reduction rate and interval time, respectively. To assess instrument reproducibility, Brownian motion of particles was measured in an Intralipid (Liposyn III, Abbott Laboratories, Chicago, IL) phantom (1%) with known reduced scattering coefficient ($\mu_s' = 10$ cm^{-1}) and absorption coefficient ($\mu_a = 0.02$ cm^{-1}; ref. 32) at 785 nm. The coefficient of variation of multiple measurements ($n = 10$) with multiple separations (1-3.5 mm) was <3%.

Broadband diffuse reflectance spectroscopy. To quantify tissue optical properties and determine tissue hemoglobin oxygen saturation (SO$_2$), broadband reflectance spectrometric measurements were made at times 15 minutes before PDT and 20 minutes, 3, and 6.5 hours after PDT. The broadband reflectance spectrometer collected reflectance spectra, determined by tissue scattering and absorption, at many source-detector separations. Based on the absorption data, tissue concentrations of chromophores such as oxyhemoglobin (HbO$_2$) and deoxyhemoglobin (Hb) were calculated. This instrument has been described in detail in recent publications (33, 34). Briefly, the system consists of a 250-W quartz tungsten halogen lamp (Cuda Fiberoptics, Jacksonville, FL), a hand-held surface contact fiber optic probe, a spectrograph (SpectraPro-150, Acton Research, Acton, MA), and a liquid nitrogen–cooled CCD camera (LN/CCD-1100-PF/UV, Roper Scientific, Trenton, NJ) to image the reflectance spectra from multiple detection fibers simultaneously. The fiber optic probe consisted of a 400-µm-diameter source fiber and 10 colinear 400-µm-diameter detection fibers at various source-detector separation distances. Due to poor signal at larger source-detector separation distances and failure of the diffusion model at very small source-detector separation distances, only signals from the detection fibers with the second and third shortest source-detector separation distances, 1.2 and 1.8 mm, were used in our algorithm to calculate tumor optical and physiologic properties, including HbO$_2$ and Hb. From this information, the total hemoglobin concentration (THC = $c_{HbO2} + c_{Hb}$) and the tissue hemoglobin oxygen saturation (SO$_2$ = c_{HbO2}/THC) were calculated. SO$_2$ typically had a coefficient of variation of <1.5% in a single location and ∼2% to 7% when averaged over the whole tumor. The latter is a function of both instrument-introduced variability (<1.5%) and heterogeneous oxygen distribution within the measured tissue (tumor). In previous studies, the broadband reflectance spectrometer was validated through the creation of the Hill curve for a tissue phantom of human or mouse erythrocytes over the course of its deoxygenation. The difference between the smoothed fit to the measured oxygen dissociation curve and published values was <5% (33, 34).

Power Doppler Ultrasound Imaging. Power Doppler ultrasound imaging of tumor perfusion was done with a broadband 12-5 MHz transducer using a Philips ATL 5000 (Philips ATL, Bothell, WA) ultrasound scanner. Imaging was done under ketamine/xylazine anesthesia (150/10 mg/kg) at times 15 minutes before, 15 minutes after, 3 hours after, and 6.5 hoursafter PDT; mice were kept warm on a heating pad. Over a period of 5 to 10 minutes, ∼10 images were acquired of each tumor. The pulse repetition frequency, color gain, and wall filters were held constant for all images. In power Doppler images, tissue regions with blood flow are coded in color. The hue, brightness, and value of the color represent the strength of the Doppler signal and are related to the concentration of the moving RBC. The color level is expressed in arbitrary units from 0 to 100, where the values 0 and 100 represent no power Doppler signal and maximum power Doppler signal, respectively. On each image, the tumor was identified and outlined as the region of interest based on a grayscale scan. Within the region of interest, the color-weighed fractional area was calculated as the product of the fractional area (ratio of colored to total pixels in the image) and the mean color level (the sum of the integrated power values divided by the number of colored pixels) as described earlier (35, 36). The average color-weighed fractional area was calculated from all images for each mouse at each time point and studied as a measure of tumor perfusion. Because mean color level represents RBC flux and fractional area covered by the colored pixels represents the area of perfusion, the product of the two is proportional to the blood volume moving through the image plane.

Statistics. Statistical analyses were carried out using R v.1.70 (free software, http://www.r-project.org) and Microsoft Excel 2000. For descriptive purposes, figures display means and SEs or SDs based on the individual data collected at each time point. However, for the purposes of statistical testing, we used SEs based on data modeled over all time points using the methods described below. Mixed effects models were used to compare blood flow patterns in animals measured by DCS versus power Doppler (37). The mixed effects model is an analysis of variance in the sense that it accounts for multiple

experimental factors as well as allowing for correlations between repeated measurements on the same animal. For the comparison of DCS and power Doppler, the model included time, modality (power Doppler versus DCS), and treatment (control versus PDT) as main effects and included interaction terms between time and treatment to allow the effect of PDT to differ over time. Based on the Akaike Information Criteria, separate random effects were used to model the interanimal variance for animals measured with power Doppler and DCS, with a common random error term to model the intra-animal variance (37). Separate analyses were also carried out to assess the effects of time and treatment on SO_2 and rBF. Likelihood ratio tests were used to assess the significance of the differences in SEs among power Doppler and DCS-measured animals and to assess the significance of the grouping factors (e.g., DCS versus power Doppler and PDT versus control; ref. 38). We used the results from the model to estimate average outcome for each time point for control and PDT-treated animals and as the basis of a Wald test comparing variables (rBF and SO_2) at individual time points to their baseline. All tests were two sided and used a type I error rate of 0.05.

The association between rBF and SO_2 or time-to-400 mm^3 was assessed for the best-fit model (linear, log, or exponential), as determined by the correlation coefficient (r^2). The statistical significance of this association was determined by a Wald test comparing the slope of the model to a slope of zero.

The Wilcoxon rank sum test was used to compare rBF or treatment durability between animals with and without hydralazine.

Results

Diffuse correlation spectroscopy and power Doppler ultrasound measure similar changes in relative blood flow after photodynamic therapy. DCS measurement of tumor blood flow was validated through comparison with power Doppler measurement of moving blood volume in tumors treated with the same PDT treatment conditions (5 mg/kg Photofrin, 135 J/cm^2, 75 mW/cm^2). Data from both instruments were expressed as the rBF (i.e., as a percentage of the baseline value measured over the 10 minutes before PDT). Figure 2 shows that DCS and power Doppler ultrasound detected similar changes in tumor blood flow at times 15 minutes, 3, and 6.5 hours after control (Fig. 2A) or PDT (Fig. 2B) treatment. The model-based estimate of the mean difference between rBF measured by DCS versus power Doppler was 11.5% (95% confidence interval, −19.0 to 42.0), a difference which was not statistically significant ($P = 0.45$) and which suggested overall good agreement between the averages estimated by the two modalities.

Tumor blood flow fluctuates significantly during photodynamic therapy. Compared with power Doppler, DCS offers the advantage of continuous blood flow monitoring during the delivery of the 630-nm illumination for Photofrin-PDT. Using DCS, relative blood flow was measured continuously beginning 10 minutes before the start of PDT until 15 minutes after the conclusion of PDT. Rapid changes in rBF were detected over the course of the 30-minute PDT treatment. Averaged traces of rBF during control or PDT treatment of animals are shown in Fig. 3. In unphotosensitized controls (Fig. 3A), minor fluctuations in rBF were detected during illumination. In PDT-treated animals (Fig. 3B), a rapid increase in rBF occurred during the first 10 minutes of treatment, peaking at 168.1 ± 39.5% (average ± SE) of the baseline. This increase was remarkably consistent among animals, and the peak occurred within the first ~1 to 10 minutes of treatment (range, 0.9-10.5 minutes). Following its PDT-induced increase, rBF decreased to 59.2 ± 29.1%
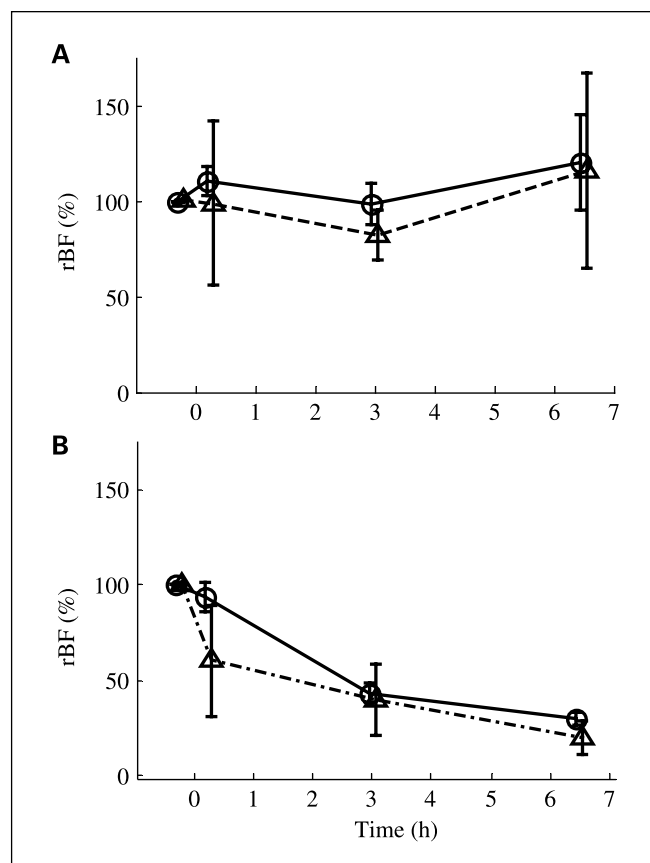
Fig. 2. rBF measured by DCS (○) and power Doppler ultrasound (△) at 15 minutes, 3, and 6.5 hours after control (*A*) or PDT (*B*) treatment. Photofrin-PDT done to 135 J/cm^2 at 75 mW/cm^2; controls received illumination, but no Photofrin. rBF at each time point was calculated as the percentage of the baseline value, measured in the same animal over the 15 minutes before PDT. Points, average; bars, ±SE. Fifteen treated and 10 control animals were evaluated by DCS; five treated and 5 control animals were evaluated by power Doppler (at 3 hours, only four animals were available).

(average ± SE) of baseline. On average, the first minimum was reached at 16 minutes after the start of treatment, but the time to the trough varied widely among tumors (range, 4.0-24.2 minutes). Tumors that reached this first trough at shorter times after the beginning of treatment tended to exhibit subsequent distinctive peaks and declines in rBF. However, these additional peaks were of a smaller magnitude than the initial increase in rBF. Representative examples of a tumor that showed a single peak in rBF versus one that showed three peaks are shown in Fig. 3C and D, respectively.

To characterize the PDT-induced changes in rBF during illumination, the following variables were defined: the maximum differential flow ($rBF_{max} - rBF_{min}$), interval time ($T_{min} - T_{max}$), and flow reduction rate (maximum differential flow / interval time). Here the rBF_{max} and rBF_{min} are the maximum and minimum flow of the first peak, respectively (see Fig. 3C and D). T_{min} and T_{max} are the time points when flow reaches the rBF_{max} and rBF_{min}. Analysis of animals with multiple peaks in rBF was based on the first peak because it was the most consistent, as well as generally the highest. In PDT-treated animals, maximum differential flow ranged from 61.8% to 137.1%, interval time ranged from 2.2 to 15.6 minutes, and flow reduction rate ranged from 4.4 to 45.8 minute^{-1}. Thus, substantial variability was
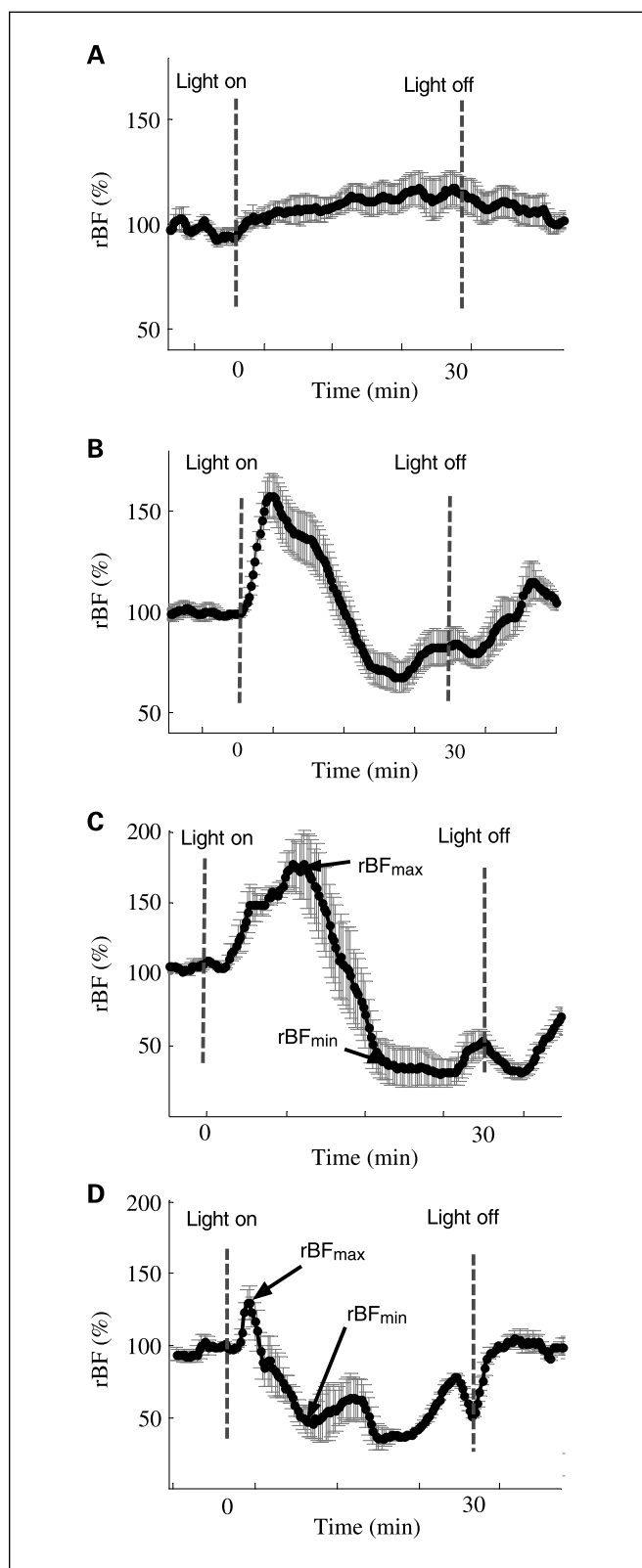
Fig. 3. Averaged traces of rBF during illumination of 10 control (*A*) and 15 PDT-treated mice (*B*) and representative traces of blood flow in PDT-treated tumors with a single (*C*) or multiple peaks (*D*) in flow. Photofrin-PDT done to 135 J/cm^2 at 75 mW/cm^2; controls received illumination, but no Photofrin. rBF was calculated as the percentage of the baseline value, measured in the same animal over the 15 minutes before PDT. Points, average; bars, ±SE (*A* and *B*) or ±SD (*C* and *D*). rBF$_{max}$ and rBF$_{min}$ are the maximum and minimum, respectively, of the first peak in blood flow.

found in the dynamics of vascular responses to PDT among animals treated with the same protocol. We expected decreases in tumor blood flow during PDT to be treatment limiting as a consequence of accompanying decreases in oxygen supply. To test this hypothesis, the association between vascular response during Photofrin-PDT and the long-term response of animals to treatment was evaluated.

Blood flow dynamics during photodynamic therapy predict treatment durability. Radiation-induced fibrosarcoma–bearing animals were monitored for rBF during PDT and followed for the durability of treatment response, measured as the time for tumor growth to a volume of 400 mm^3 (time-to-400 mm^3). No association was detected between starting tumor volume and time-to-400 mm^3 in controls (mean volume ± SE, 103.1 ± 6.1 mm^3; $P = 0.31$, $r^2 = 0.13$) or PDT-treated animals (mean volume ± SE, 109.1 ± 13.3 mm^3; $P = 0.70$, $r^2 = 0.01$). In control animals, time-to-400 mm^3 was highly consistent and ranged from only 3 to 6 days. In contrast, time-to-400 mm^3 ranged from 7 to 24 days in the PDT-treated animals. In these animals, the relationship between time-to-400 mm^3 and tumor blood flow dynamics during PDT, characterized by flow reduction rate, maximum differential flow, and interval time was explored.

The association between flow reduction rate and treatment durability is plotted in Fig. 4A. Flow reduction rate was highly
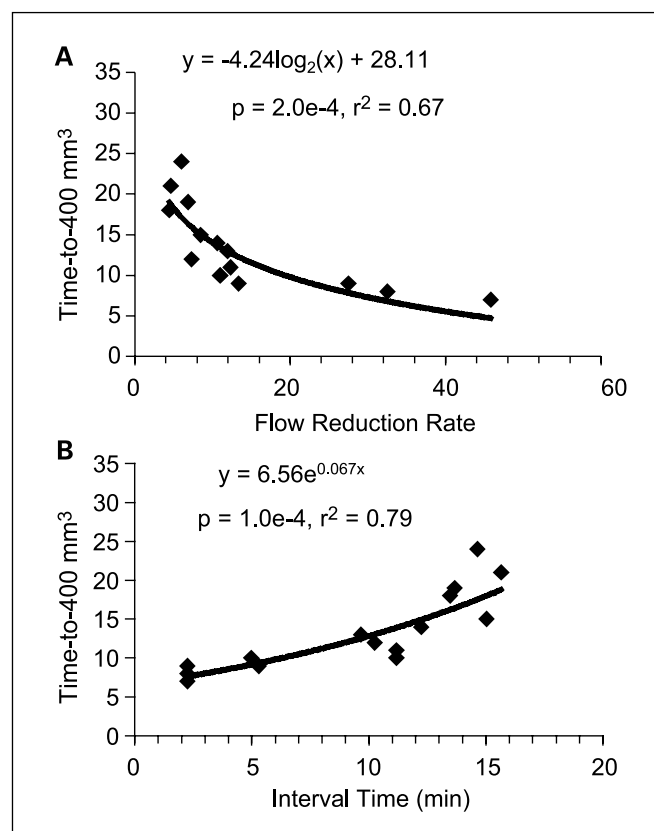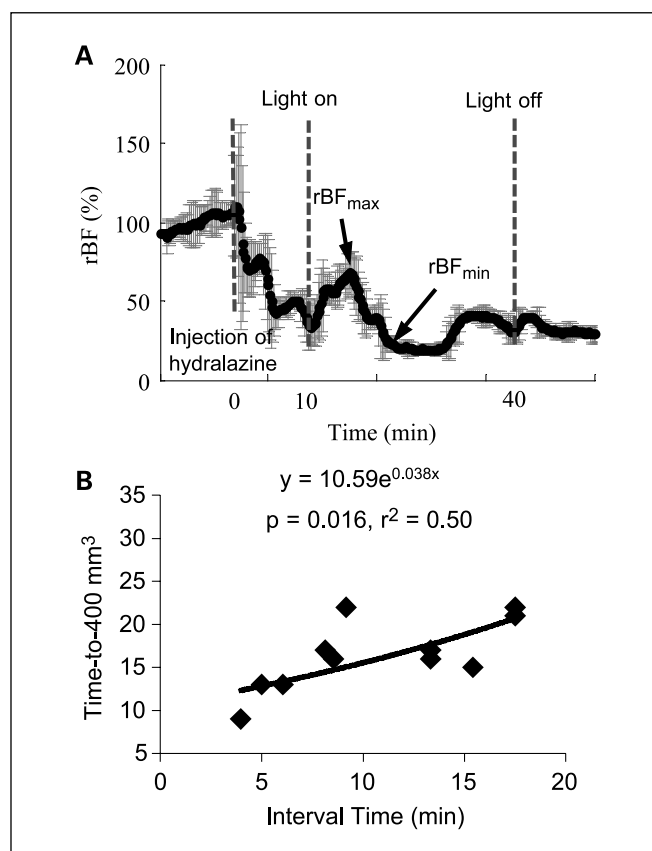

Fig. 4. Correlation between treatment durability (time-to-400 mm^3) and flow reduction rate (*A*) or interval time (*B*) during PDT. Flow reduction rate is the slope of the decrease in blood flow after its initial PDT-induced increase, and interval time is the time difference between rBF$_{max}$ and rBF$_{min}$ (see Fig. 3). Animals (*n* = 15) received Photofrin-PDT to 135 J/cm^2 at 75 mW/cm^2. SE in flow reduction rate and interval time ranged from 0.3 to 5.6 (median = 0.6) and 0.1 to 0.6 (median = 0.4), respectively.

correlated with time-to-400 mm^3 (P = 0.0002, r^2 = 0.67), whereby tumors with rapid decreases in rBF during PDT (higher values of flow reduction rate) showed shorter growth delays after treatment. A doubling of flow reduction rate during PDT led to a decrease in the time-to-400 mm^3 by 4.2 ± 0.8 days (average ± SE). Flow reduction rate is the slope of the decrease in rBF during PDT and defined as maximum differential flow / interval time. The association between flow reduction rate and treatment durability was a function of interval time but not of maximum differential flow. The interval time (Fig. 4B) was significantly correlated with tumor time-to-400 mm^3 (P = 0.0001) and displayed a better fit to its model than the association between flow reduction rate and time-to-400 mm^3 (r^2 = 0.79 versus 0.67, respectively). A 10-minute increase in interval time was associated with a 6.28 ± 1.16 day increase (average ± SE) in the time-to-400 mm^3. No association (P = 0.89, r^2 = 0.1) between maximum differential flow and time-to-400 mm^3 was detected.

Blood flow dynamics during photodynamic therapy of tumors with altered pretreatment flow. To assess the value of blood flow monitoring during PDT in the presence of altered baseline flow, animals were injected with the vasodilating drug hydralazine at 10 minutes before illumination. Two injected doses of hydralazine were tested, 2.5 and 5 mg/kg. Hydralazine moderately decreased tumor rBF (discussed in more detail below) but failed to affect the overall tumor response; time-to-400 mm^3 ranged from 9 to 22 days in PDT-treated, hydralazine-dosed animals, compared with 7 to 24 days in animals treated with the same PDT protocol in the absence of hydralazine. Hydralazine injection also failed to affect the response of controls (range, 2-5 days in time-to-400 mm^3). A sample trace of tumor rBF from 10 minutes before hydralazine injection through 15 minutes after PDT is shown in Fig. 5A. On average, hydralazine at 2.5 mg/kg resulted in rBF reduction to 60% at 10 minutes after injection, whereas an injected dose of 5 mg/kg resulted in rBF reduction to 49%. After beginning PDT, rBF increased slightly and declined; hydralazine dose had no effect on the magnitude or timing of PDT-induced changes on rBF. As found in the previous study (no hydralazine administration), interval time was significantly correlated (P = 0.016, r^2 = 0.50) with tumor time-to-400 mm^3 (Fig. 5B) in animals that received hydralazine and PDT. Also similar to the results of the previous study, flow reduction rate was not as strong as interval time in its predictive power. The flow reduction rate approached (P = 0.08) but did not achieve statistical significance in its association with time-to-400 mm^3 in the hydralazine-treated animals.

Relative blood flow and oxygenation of tumors decrease after photodynamic therapy. PDT-induced changes in tumor blood flow were followed for up to 6.5 hours after completion of treatment. rBF progressively decreased with time after PDT in treated mice (see Fig. 2B) but was relatively stable in control animals (see Fig. 2A). Over time, differences between the control and PDT-treated groups were statistically significant (P < 0.0001). In the PDT-treated animals, rBF measured by DCS at 15 minutes after the conclusion of PDT was 93.8% of its baseline (P = 0.44). However, by 3 hours after PDT, rBF significantly decreased (P < 0.0001) to 43.7% of the baseline value. A slightly greater reduction was found at 6.5 hour after PDT, when average rBF was 30.2% (P < 0.0001) of its baseline value. The SE for each average based on data from all the time points was 7.8%.

Fig. 5. Representative trace of rBF in the tumor of an animal treated with hydralazine (2.5 mg/kg, i.v.) 10 minutes before Photofrin-PDT to 135 J/cm^2 at 75 mW/cm^2 (*A*). Points, average; bars, ±SD. Correlation between treatment durability (time-to-400 mm^3) and interval time in animals receiving hydralazine (2.5 or 5 mg/kg, i.v.) and Photofrin-PDT to 135 J/cm^2 at 75 mW/cm^2 (n = 11; *B*). Interval time is the time difference between rBF$_{max}$ and rBF$_{min}$. SE in interval time ranged from 0.1 to 0.5 (median = 0.3).

Changes in other tumor physiologic variables may be expected to accompany the decreases in blood flow after PDT. Specifically, we measured tissue hemoglobin oxygen saturation (SO$_2$) of the same tumors followed for blood flow. In the PDT-treated animals, average tumor SO$_2$ at 15 minutes before PDT was 35.7%. The SO$_2$ increased slightly to 47.2% at 20 minutes after PDT (P = 0.022) and decreased to 19.7% and 8.4% at 3 and 6.5 hours after PDT, respectively (Fig. 6). The decreases in SO$_2$ at 3 and 6.5 hours after PDT were also both significant relative to the pre-PDT value (P = 0.0018 and P < 0.0001, respectively). The SE for each average, based on data from all the time points was 4.5%. In unphotosensitized, light-treated control animals the average SO$_2$ ranged from 26.2% to 29.4% across all time points; no differences across time were detected and the SE of the estimate was 5.5%. Differences in patterns of mean SO$_2$ over time between control and PDT-treated groups were highly significant (P < 0.0001).

Relative blood flow and oxygenation of tumors after photodynamic therapy predict treatment durability. Decreases in rBF and SO$_2$ at 3 and 6.5 hours after PDT are consistent with the progressive development of PDT-induced vascular damage, leading to tumor cell death. The association between delayed PDT vascular effects and the durability of tumor response (time-to-400 mm^3) was evaluated (Fig. 7). A highly significant
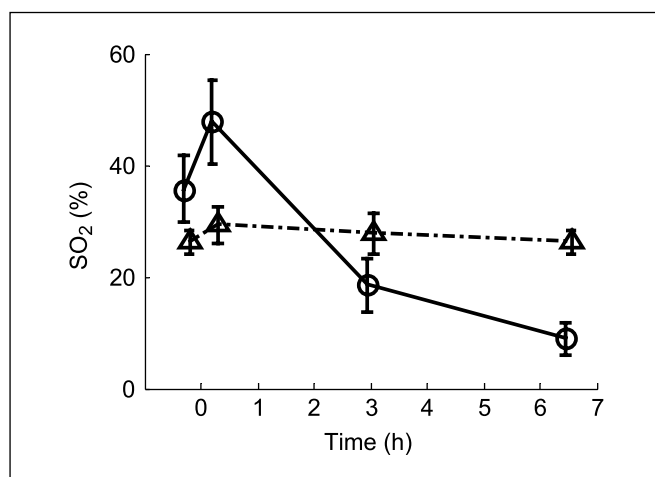
Fig. 6. SO_2 after PDT in treated (○) and control (△) mice. SO_2 is the absolute value measured by broadband diffuse reflectance spectroscopy. Points, average; bars, ±SE. Photofrin-PDT done to 135 J/cm² at 75 mW/cm². Ten controls and 15 PDT-treated animals were evaluated (at 20 minutes, 3, and 6.5 hours, only 14 PDT-treated mice were available).

negative correlation ($P < 0.0001$, $r^2 = 0.8$) was detected between rBF at 3 hours after PDT and tumor time-to-400 mm³ (Fig. 7A). This association indicates that tumors with larger reductions in rBF after PDT require more time for growth. A model describing these data indicates that a doubling of the rBF at 3 hours after PDT leads to a 7.00 ± 0.95 day (average ± SE) decrease in tumor time-to-400 mm³. rBF at 6.5 hours after PDT was also highly correlated ($P < 0.0001$, $r^2 = 0.75$) with tumor response (data not shown). A model of the effect at 6.5 hours indicates that a doubling of the rBF leads to a 5.86 ± 0.94 day decrease in time-to-400 mm³, very similar to that found at 3 hours.

Tumor SO_2 at 3 hours after PDT was also predictive ($P = 0.015$, $r^2 = 0.40$) of tumor response (Fig. 7B); as expected, decreasing tumor SO_2 was associated with increasing tumor time-to-400 mm³. A model of these data indicates that for each 1% increase in SO_2 the time-to-400 mm³ was reduced by 0.17 days. Accordingly, an increase in tumor SO_2 from 0% to 10% at 3 hour after PDT resulted in a 1.70 ± 0.56 day decrease in treatment durability. The effect of tumor SO_2 at 6.5 hours after PDT on time-to-400 mm³ was not modeled because half of the available data (7 of 14 animals) had a value of "zero".

Animals that received hydralazine were also evaluated for an association between rBF at 3 hours after PDT and treatment durability. Hydralazine injection resulted in significant ($P = 0.005$) decreases in rBF at 3 hours compared with that in mice treated with PDT alone (rBF range, 12-44% and 19-79%, respectively). No association between treatment durability and rBF at 3 hours after PDT in hydralazine-treated mice was detectable.

Blood flow dynamics during photodynamic therapy predict vascular responses to treatment. PDT effects on tumor rBF both during and after treatment were individually predictive of the tumor response. This led us to investigate the presence of an association between rBF during PDT and the development of delayed vascular damage, measured by changes in rBF after PDT. The correlation between rBF at 3 hours after PDT and interval time during PDT is plotted in Fig. 8. These data were highly correlated ($P = 0.0003$, $r^2 = 0.75$), whereby increasing
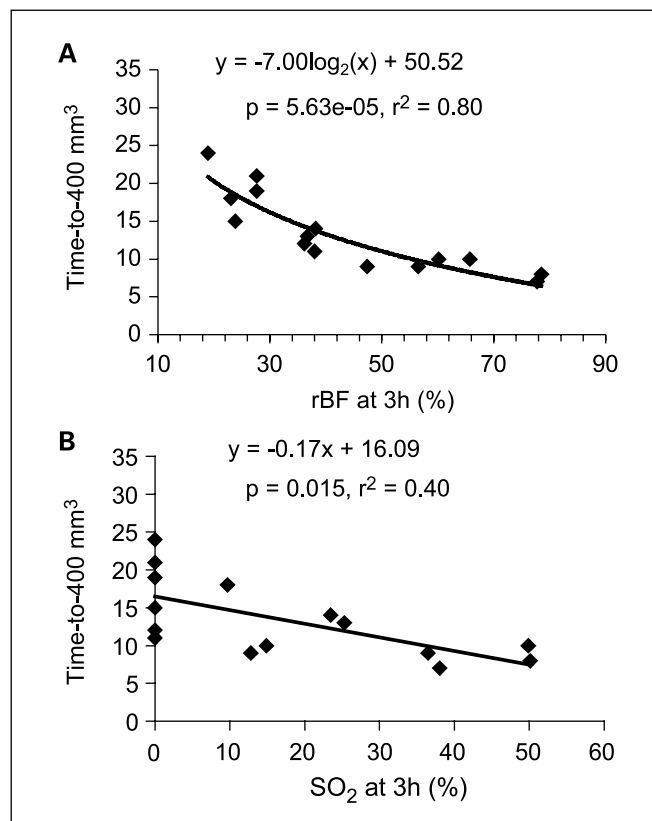

Fig. 7. Correlation between treatment durability (time-to-400 mm³) and rBF (*A*) or SO_2 (*B*) at 3 hours after PDT ($n = 15$). Photofrin-PDT done to 135 J/cm² at 75 mW/cm². A linear-to-log regression was used to test for an association between treatment efficacy and rBF, whereas a linear regression was used to test for an association between treatment efficacy and SO_2 because the latter data contained many "zeros". SD ranged from 0.8 to 13.7 (median = 3.9) in rBF and from 0 to 50.1 (median = 14.9) in SO_2, reflecting a highly heterogeneous tumor microenviroment at this time point.

interval time predicted for larger decreases in rBF at 3 hours. Similarly, interval time was correlated with rBF at 6.5 hours after PDT ($P = 0.00028$, $r^2 = 0.65$) and with SO_2 at 3 hours after PDT ($P = 0.027$, $r^2 = 0.35$; data not shown).

Discussion

The antivascular effects of Photofrin-mediated PDT have been well studied (39), and many second generation photosensitizers also create prominent vascular responses (40). Methods, both invasive and noninvasive, for investigating vascular damage during or after PDT include intravital microscopy (39, 40), laser Doppler (17, 41), power Doppler, and optical coherence tomography (19). The study of tumor blood flow during PDT has been technically challenging, especially by noninvasive methods. In the present study, we show that DCS can be used to follow changes noninvasively in tumor rBF during and after PDT. The relevance of these measurements was shown by correlative studies of the association between rBF and treatment durability (time-to-400 mm³). Overall, these data show the utility of DCS for monitoring PDT-created changes in the rBF of tumors and the potential dosimetric value of such measurements. Translation of this technology to the clinic could, in some instances, require modification of the
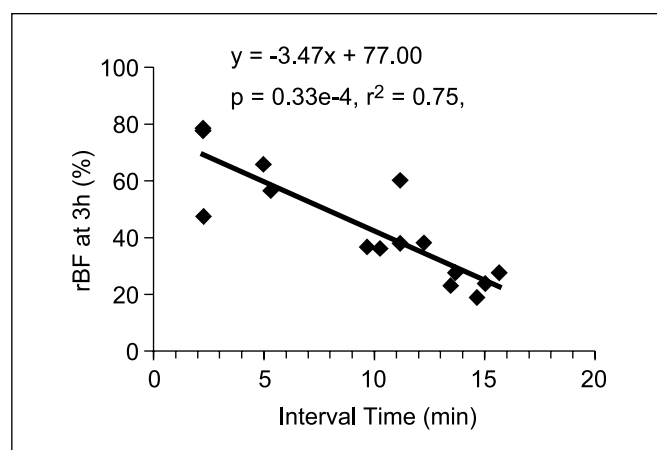
Fig. 8. Correlation between rBF at 3 hours after PDT and interval time during PDT. Interval time is the time difference between rBF_{max} and rBF_{min} (see Fig. 3). Animals ($n = 15$) received Photofrin-PDT to 135 J/cm^2 at 75 mW/cm^2.

probe-tissue interface. For example, a fiber-bundled probe consisting of source and detector fibers can be used for monitoring of tumor blood flow responses during interstitial PDT applications.

Monitoring of blood flow by DCS has been studied extensively in normal tissue such as brain and muscle (22–24, 28). In the present report, DCS technology with a unique noncontact probe was used to measure rBF in murine tumors. The near-IR illumination used for DCS enables the measurement of tissue depths up to 15 mm (24, 28); however, source-detector separation determines the depth of tissue sampled. Source-detector distances ranging from 1 to 3.5 mm were used for tumors in this study, providing blood flow data from a depth of 0.5 to 1.7 mm. This distance places the measurements below the murine skin and well into the tumor, deeper than that achieved by other optical techniques. It offers the advantage of measuring a relatively central slice of tumor with minimum contribution of signal from the overlying skin or underlying muscle. Furthermore, measurement of greater tumor depths is possible in tumors of larger size that can accommodate more widely spaced source-detector distances. Validation of DCS measurement of radiation-induced fibrosarcoma tumor oxygenation after PDT was provided by comparison with tumor perfusion measured by power Doppler ultrasound in animals treated with identical PDT conditions. The two methods detected similar rBF after PDT or light treatment with a mean difference of 11.5%, which was not statistically significant ($P = 0.48$). Furthermore, decreases in rBF to 43.7% and 30.2% at 3 and 6.5 hours after PDT were closely reflected by decreases in tumor oxygenation (SO$_2$) to 52.2% and 23.5% of the baseline value, measured by broadband reflectance spectroscopy at respective time points.

One limitation of DCS hemodynamic measurements is the difficulty in quantifying absolute blood flow levels. Data presented are rBF, calculated as blood flow at the time point of interest normalized to the pre-PDT flow. Nevertheless, the present data indicate rBF measurement is sufficient and even possibly the preferred method for monitoring of PDT responses. To characterize blood flow during PDT, we calculated the time over which blood flow decreased to a minimum after the first PDT-induced peak in flow (interval

time). Because all animals were treated with the same PDT fluence and fluence rate, the time (in minutes) provided a rational means of comparing among animals. Alternative variables, such as the fluence range over which blood flow decreases or the percentage of the total treatment encompassed by the decrease potentially could be valuable for comparisons among animals receiving different treatments.

A distinct advantage of DCS is the ability to monitor rBF noninvasively over the course of PDT. Few others have followed blood flow during PDT. Studies by Pogue et al. (17) using laser Doppler between light fractions detected PDT-induced average decreases in blood flow; however, values for individual animals were not reported. Fingar et al. (39) used intravital microscopy to measure constriction of the arteries of rat muscle treated with Photofrin-PDT. They divided vasoresponses into two categories: vessels that remained constricted through at least 1 hour after PDT and vessels that showed relaxation during or shortly after treatment. Our data indicate an initial treatment-induced increase in tumor rBF followed by a reduction in rBF and subsequent peaks and declines. Oscillations of the same magnitude were not found in the rBF of light-treated control animals, and only small increases in tumor temperature (<1.5°C) were measured during PDT. We suggest transient increases in rBF upon illumination may be a physiologic response to hypoxia created by photochemical oxygen consumption. It is well known that hypoxia initiates vasodilation in the systemic arteries of normal tissues (42). In tumors receiving PDT, treatment-created increases in rBF may be accompanied by the production of reactive oxygen species at the vascular endothelium, leading to vasoconstriction. Resulting limitations to the oxygen supply may offer vessels protection from continuing photochemical damage, thus facilitating a possible recovery in blood flow. The kinetics of changes in tumor oxygenation versus blood flow during PDT are best determined by direct measurement of both variables during illumination; we are currently developing technology capable of such measurements.

Previous investigations of PDT antivascular effects have compared the average vascular response of one group of animals with the tumor response of a separate group, treated with the same condition (7, 8, 13). The value of hemodynamic monitoring in the same animal subsequently followed for tumor response has been little tested. Thus, we sought to show the potential therapeutic usefulness of noninvasive blood flow measurements as a tool to predict treatment efficacy. Tumor rBF at both 3 and 6.5 hours after PDT was significantly associated with treatment durability. Tumor SO$_2$ at 3 hours after PDT also predicted tumor response, independent of data on rBF. As to be expected, tumors with more severe PDT-created declines in rBF or SO$_2$ exhibited a longer delay in growth.

To study the association between tumor blood flow during PDT and treatment response we characterized rBF during PDT by the duration (interval time) and slope (flow reduction rate) of its decline after the initial PDT-induced peak in flow. The length of this decline in rBF was variable among animals, with the minimum value reached between 4 and 24 minutes after the beginning of treatment. Those animals with slower declines in rBF, characterized by a larger interval time and smaller flow reduction rate, showed a more durable treatment response. Furthermore, these animals also had enhanced post-treatment vascular shutdown, determined via rBF and SO$_2$ measurement

at 3 hours after PDT conclusion. These findings are consistent with the hypothesis that treatment efficacy is a function of tumor oxygenation during PDT: under oxygen-limiting conditions (i.e., rapidly declining blood flow), treatment efficacy was abrogated. Although tumors with rapid declines in rBF commonly exhibited subsequent peaks, these peaks were small in magnitude relative to the initial increase in rBF and likely provided limited benefit to tumor oxygenation.

Further testing of the value of hemodynamic monitoring during PDT was done in animals with significantly depressed pre-PDT blood flow due to administration of the vasodilating drug hydralazine. As shown by others (43), we found hydralazine to reduce tumor blood flow, likely through a "steal" effect following systemic drug-induced vasodilation. However, hydralazine itself did not significantly affect the durability of the PDT tumor response. The failure of a pre-PDT decrease in blood flow to affect treatment durability can be explained in several ways. First, others have also shown that mild pretreatment hypoxia induced by vasoactive drugs fails to abrogate long-term PDT tumor response (44). Second, DCS measurements show an average decrease of 40% to 50% in the blood flow of hydralazine-treated mice; however, the absolute value of the blood flow measurement was not measured. It is surely possible that the absolute value of blood flow in poorly perfused tumors that didn't receive hydralazine was similar to well-perfused tumors that did receive hydralazine, even after a 40% decrease in flow. Such overlap is not visible in our measurements because we necessarily report values relative to that found pretreatment (either PDT or hydralazine), yet it would clearly affect the differential in absolute tumor response (measured as treatment durability) between the hydralazine-treated and hydralazine-free groups. Finally, it is relevant to note that even during PDT the magnitude of the change in blood flow ($rBF_{max} - rBF_{min}$; i.e., maximum differential flow) was not associated with treatment durability; this is consistent with the observation that a change in the magnitude of blood flow before PDT did not strongly affect tumor response.

Despite depressed pre-PDT blood flow in hydralazine-treated mice, the PDT-induced change in rBF (interval time) remained predictive of tumor response, in excellent agreement with the strong correlation between interval time and PDT response in hydralazine-free animals. In other words, interval time in mice given hydralazine was in the same range (~5-18) as interval time in PDT-treated mice not exposed to hydralazine (~2-16); consequently, DCS measurements predict, and are correct in their prediction, that the two groups of animals should exhibit similar tumor responses. These findings suggest that PDT effect on blood flow during illumination may be more informative of tumor response than level of preexisting flow (presumably above a minimum threshold). It agrees with our recent finding that the normalized change in radiation-induced fibrosarcoma tumor oxygenation (SO_2) immediately after to before Photofrin-PDT is a stronger predictor of the tumor response than preexisting oxygen levels (33).

In animals that received hydralazine, no association between rBF at 3 hours after PDT and treatment durability could be detected. This is in stark contrast to the strong association between rBF at 3 hours after PDT and treatment response in animals free of hydralazine. Hydralazine-dosed animals showed significantly greater reductions in rBF at 3 hours after PDT than did animals that received PDT alone. This effect seems a consequence of the added insult of PDT after hydralazine administration because hydralazine-dosed, light-treated control animals showed full blood flow recovery by 3 hours after illumination (average rBF ± SE = 105.2 ± 15.9%). Thus, at the 3-hour time point, it is not possible to separate the effects of PDT versus those of hydralazine on rBF; yet, it is known that hydralazine plus PDT did not significantly enhance tumor response compared with PDT alone. The contribution of hydralazine to rBF responses at 3 hours, in the absence of any accompanying effect on a long-term tumor response, confounds any attempt to correlate these variables.

In conclusion, we have shown that near-IR diffuse correlation spectroscopy can be used to monitor tumor rBF noninvasively during and after photodynamic therapy. PDT-induced changes in rBF during treatment were significantly associated with subsequent decreases in rBF and SO_2 in the hours after PDT. Furthermore, each of these variables, rBF during PDT, rBF after PDT, and SO_2 after PDT, individually predicted treatment durability. Similar studies using different PDT photosensitizers are ongoing. However, many photosensitizers exhibit a vascular component to PDT response, suggesting a potential role for blood flow monitoring as tool for real-time PDT treatment planning or rapid (within hours) efficacy assessment. This research suggests that DCS measurements of blood flow are potentially useful for clinical PDT trials.

Acknowledgments

References

1. Dougherty TJ, Gomer CJ, Henderson BW, et al. Photodynamic therapy. J Natl Cancer Inst 1998;90: 889–905.

2. Oleinick NL, Morris RL, Belichenko I. The role of apoptosis in response to photodynamic therapy: what, where, why, and how. Photochem Photobiol Sci 2002;1:121.

3. van Duijnhoven FH, Aalbers RI, Rovers JP, Terpstra OT, Kuppen PJ. The immunological consequences of photodynamic treatment of cancer, a literature review. Immunobiology 2003;207:105–13.

4. Chen B, Pogue BW, Goodwin IA, et al. Blood flow dynamics after photodynamic therapy with verteporfin in the RIF-1 tumor. Radiat Res 2003;160:452–9.

5. Chan WS, Brasseur N, La Madeleine C, van Lier JE. Evidence for different mechanisms of EMT-6 tumor necrosis by photodynamic therapy with disulfonated aluminum phthalocyanine or Photofrin: tumor cell survival and blood flow. Anticancer Res 1996;16: 1887–92.

6. Fingar VH, Wieman TJ, Karavolos PS, Doak KW, Ouellet R, van Lier JE. The effects of photodynamic therapy using differently substituted zinc phthalocyanines on vessel constriction, vessel leakage and tumor response. Photochem Photobiol 1993;58: 251–8.

7. McMahon KS, Wieman TJ, Moore PH, Fingar VH. Effects of photodynamic therapy using mono-L-aspartyl chlorin e6 on vessel constriction, vessel leakage, and tumor response. Cancer Res 1994;54: 5374–9.

8. Fingar VH, Kik PK, Haydon PS, et al. Analysis of acute vascular damage after photodynamic therapy using benzoporphyrin derivative (BPD). Br J Cancer 1999; 79:17028.

9. van Geel IP, Oppelaar H, Rijken PF, et al. Vascular perfusion and hypoxic areas in RIF-1 tumours after photodynamic therapy. Br J Cancer 1996;73:288–93.

10. Busch TM, Wileyto EP, Emanuele MJ, et al. Photodynamic therapy creates fluence rate-dependent gradients in the intratumoral spatial distribution of oxygen. Cancer Res 2002;62:7273–9.

11. Sitnik TM, Hampton JA, Henderson BW. Reduction of tumour oxygenation during and after photodynamic therapy *in vivo*: effects of fluence rate. Br J Cancer 1998;77:1386–94.

12. Fingar VH, Siegel KA, Wieman TJ, Doak KW. The effects of thromboxane inhibitors on the microvascular

and tumor response to photodynamic therapy. Photochem Photobiol 1993;58:393–9.

13. Henderson BW, Sitnik-Busch TM, Vaughan LA. Potentiation of photodynamic therapy antitumor activity in mice by nitric oxide synthase inhibition is fluence rate dependent. Photochem Photobiol 1999; 70:64–71.

14. Busch TM, Hahn SM, Evans SM, Koch CJ. Depletion of tumor oxygenation during photodynamic therapy: detection by the hypoxia marker EF3 [2-(2-nitroimidazol-1[*H*]-yl)-*N*-(3,3,3-trifluoropropyl)-acetamide]. Cancer Res 2000;60:2636–42.

15. Wang L, Cull G, Cioffi GA. Depth of penetration of scanning laser Doppler flowmetry in the primate optic nerve. Arch Ophthalmol 2001;119:1810–4.

16. Chang HY, Chen CR, Hussain SN. Diaphragmatic microcirculation measured by laser-Doppler flowmetry in the rat. J Appl Physiol 1995;78:1225–33.

17. Pogue BW, Braun RD, Lanzen JL, Erickson C, Dewhirst MW. Analysis of the heterogeneity of *p*O$_2$ dynamics during photodynamic therapy with verteporfin. Photochem Photobiol 2001;74:700–6.

18. Tang SJ, Gordon ML, Yang VX, et al. *In vivo* Doppler optical coherence tomography of mucocutaneous telangiectases in hereditary hemorrhagic telangiectasia. Gastrointest Endosc 2003;58:591–8.

19. Chen Z, Milner TE, Wang X, Srinivas S, Nelson JS. Optical Doppler tomography: imaging *in vivo* blood flow dynamics following pharmacological intervention and photodynamic therapy. Photochem Photobiol 1998;67:56–60.

20. Bizheva K, Unterhuber A, Hermann B, et al. Imaging *ex vivo* and *in vitro* brain morphology in animal models with ultrahigh resolution optical coherence tomography. J Biomed Opt 2004;9:719–24.

21. Gee MS, Saunders HM, Lee JC, et al. Doppler ultrasound imaging detects changes in tumor perfusion during antivascular therapy associated with vascular anatomic alterations. Cancer Res 2001;61:2974–82.

22. Culver JP, Durduran T, Furuya D, Cheung C, Greenberg JH, Yodh AG. Diffuse of optical tomography cerebral blood flow, oxygenation and metabolism in rat during focal ischemia. J Cereb Blood Flow Metab 2003;23:911–24.

23. Cheung C, Culver JP, Takahashi K, Greenberg JH, Yodh AG. *In vivo* cerebrovascular measurement combining diffuse near-infrared absorption and correlation spectroscopies. Phys Med Biol 2001;46:2053–65.

24. Durduran T, Yu G, Burnett MG, et al. Diffuse optical measurement of blood flow, blood oxygenation, and metabolism in a human brain during sensorimotor cortex activation. Opt Lett 2004;29:1766–8.

25. Menon C, Polin GM, Prabakaran I, et al. An integrated approach to measuring tumor oxygen status using human melanoma xenografts as a model. Cancer Res 2003;63:7232–40.

26. Boas DA, Yodh AG. Spatially varying dynamical properties of turbid media probed with diffusing temporal light correlation. J Opt Soc Am A Opt Image Sci Vis 1997;14:192–215.

27. Yu G, Durduran T, Furuya D, et al. Hemodynamic measurements in rat brain and human muscle combining diffuse near-infrared absorption and correlation spectroscopies. Chance B, Alfano RR, Tromberg BJ, Tamura M, and Sevick-Muraca EM, editors. In: Proceedings of SPIE; 2003 Jan 26-29; San Jose (CA): SPIE; 2003. 4955: p. 164–74.

28. Yu G, Durduran T, Lech G, et al. Time-dependent blood flow and oxygenation in human skeletal muscles measured with noninvasive near-infrared diffuse optical spectroscopies. J Biomed Opt. 2005, in press.

29. Maret G, Wolf PE. Multiple light scattering from disordered media. The effect of Brownian motion of scatterers. Z Phys B 1987;65:409–13.

30. Pine DJ, Weitz DA, Chaikin PM, Herbolzheimer. Diffusing-wave spectroscopy. Phys Rev Lett 1988; 60:1134–7.

31. Boas DA, Campbell LE, Yodh AG. Scattering and imaging with diffusing temporal field correlations. Phys Rev Lett 1995;75:1855–8.

32. van Staveren HJ, Moes CJM, van Marle J, Prahl SA, van Gemert MJC. Light scattering in Intralipid-10% in the wavelength range of 400-1100 nm. Appl Opt 1991;30:4507–14.

33. Wang HW, Zhu TC, Putt ME, et al. Broadband reflectance measurements of light penetration, blood oxygenation, hemoglobin concentration, and drug concentration in human intraperitoneal tissues before and after photodynamic therapy. J Biomed Opt 2005; 10:014004.

34. Wang HW, Putt ME, Emanuele MJ, et al. Treatment-induced changes in tumor oxygenation predict photodynamic therapy outcome. Cancer Res 2004;64: 7553–61.

35. Sehgal CM, Arger PH, Rowling SE, Conant EF, Reynolds C, Patton JA. Quantitative vascularity of breast masses by Doppler imaging: regional variations and diagnostic implications. J Ultrasound Med 2000; 19:427–40; quiz 41–2.

36. Sehgal CM, Arger PH, Silver AC, et al. Renal blood flow changes induced with endothelin-1 and fenoldopam mesylate at quantitative Doppler US: initial results in a canine study. Radiology 2001;219:419–26.

37. Pinheiro JC, Bates DM. Mixed-effects models in S and S-plus. New York: Springer; 2000.

38. Harrell FE. Regression modeling strategies: with applications to linear models, logistic regression, and survival analysis. New York: Springer-Verlag; 2001.

39. Fingar VH, Wieman TJ, Wiehle SA, Cerrito PB. The role of microvascular damage in photodynamic therapy: the effect of treatment on vessel constriction, permeability, and leukocyte adhesion. Cancer Res 1992; 52:4914–21.

40. Garbo GM, Vicente MG, Fingar V, Kessel D. Effects of ursodeoxycholic acid on photodynamic therapy in a murine tumor model. Photochem Photobiol 2003; 78:407–10.

41. Kelleher DK, Thews O, Scherz A, Salomon Y, Vaupel P. Perfusion, oxygenation status and growth of experimental tumors upon photodynamic therapy with Pd-bacteriopheophorbide. Int J Oncol 2004;24:1505–11.

42. Leach RM, Hill HS, Snetkov VA, Ward JP. Hypoxia, energy state and pulmonary vasomotor tone. Respir Physiol Neurobiol 2002;132:55–67.

43. Jarm T, Podobnik B, Sersa G, Miklavcic D. Effect of hydralazine on blood flow, oxygenation, and interstitial fluid pressure in subcutaneous tumors. Adv Exp Med Biol 2003;510:25–9.

44. Fingar VH, Wieman TJ, Park YJ, Henderson BW. Implications of a pre-existing tumor hypoxic fraction on photodynamic therapy. J Surg Res 1992;53: 524–8.